

# QUANTITATIVE IMAGING OF MULTI-COMPONENT TURBULENT JETS

Ash, A., Djilali, N. and Oshkai, P.

Department of Mechanical Engineering, Institute for Integrated Energy Systems, University of Victoria, Victoria, BC V8W 3P6, Canada, arashe@uvic.ca, ndjilali@uvic.ca, poshkai@uvic.ca

## ABSTRACT

The integration of a hydrogen gas storage arrangement in vehicles has not been without its challenges. Gaseous state of hydrogen at ambient temperature, combined with the fact that hydrogen is highly flammable, results in the requirement of more robust, high pressure storage systems that can meet modern safety standards. To develop these new safety standards and to properly predict the phenomena of hydrogen dispersion, a better understanding of the resulting flow structures and flammable region from controlled and uncontrolled releases of hydrogen gas must be achieved. With the upper and lower explosive limits of hydrogen known, the flammable envelope surrounding the site of a uncontrolled hydrogen release can be found from the concentration field. In this study the subsonic release of hydrogen was emulated using helium as a substitute working fluid. A sharp orifice round turbulent jet is used to emulate releases in which leak geometry is circular. Effects of buoyancy and crossflow were studied over a wide range of Froude numbers. The velocity fields of turbulent jets were characterized using particle image velocimetry (PIV). The mean and fluctuation velocity components were well quantified to show the effect of buoyancy due to the density difference between helium and the surrounding air. In the range of Froude numbers investigated ( $Fr = 1000, 750, 500, 250$  and  $50$ ), the increasing effects of buoyancy were seen to be proportional to the reduction of the  $Fr$  number. While buoyancy is experienced to have a negligible effect on centerline velocity fluctuations, acceleration due to buoyancy in the other hand resulted in a slower decay of time-averaged axial velocity component along the centerline. The obtained results will serve as control reference values for further concentration measurement study and for computational fluid dynamics (CFD) validation.

## Nomenclature

$D$	Jet diameter
$Fr$	Froude Number
$g$	acceleration due to gravity
$L_M$	Jet/Plume characteristic length scale
$n$	Coordinate system normal to jet centerline
$Q$	Flow rate
$Re$	Reynolds Number
$s$	Coordinate system along jet centerline
$U_{oc}$	Center line velocity at jet orifice
$U_{mc}$	Maximum centerline velocity
$u'$	U velocity fluctuation
$ U $	Velocity magnitude
$v_\infty$	Cross-flow velocity
$v'$	V velocity fluctuation
$x$	Coordinate system along jet initial axis
$y$	Coordinate system along cross-flow direction
$\rho_\infty$	Ambient air density
$\rho_j$	Jet exit density of helium

## 1.0 INTRODUCTION

Prior to the development of a hydrogen infrastructure, well-researched safety standards must be implemented to reduce the risk of leaks and uncontrolled combustion related to high pressure hydrogen storage. These leaks range from slow releases from small-diameter holes in delivery pipes to high volume dispersions from accidental or controlled gas venting from high-pressure storage tanks. The resulting hydrogen jet and the combustible cloud represent a potential fire hazard. To develop new safety standards, the momentum and buoyancy effects related to the rapid, uncontrolled release of hydrogen must be studied in detail to accurately determine the resultant dispersion.

Buoyant jet discharge has been studied for over a century, which resulted in extensive knowledge and theories about the nature of these releases. Several numerical and experimental researches have been formed on these theories which have led to considerable experimental data. These studies suggest that distinct flow regions are formed in a buoyant jet release, namely, initial strong jet region, weak jet region, advected line momentum puff region, advected plume region, and the advected thermal region [1]. In each region, the flow behaviour is dominated by a set of independent flow parameter and overall behaviour of the flow is mostly independent of the initial region. Depending on the case being considered, some or all of these flow regions may occur but it should be noted that for any buoyant gas release the overall characteristics of the flow can be described by these distinct region. Large-scale ignited and unignited hydrogen leaks have been studied widely [2,3,4]. In order to characterize the hydrogen discharge scenario in downstream of the leak and also to better understand extent of flammable gas envelope, these studies were extended to small unignited leaks in regions of momentum-dominated flows (high Froude numbers) and in flows where buoyancy forces are more pronounced (low Froude numbers). These slow leaks may take place in various small-scale hydrogen based systems with leaky fittings and O-rings seals or in low pressure electrolysers as well as in vents in storage hydrogen facilities. Schefer et al. [5,6] described measurements of hydrogen dispersion in a laboratory-scale leak in cases of both momentum and buoyancy dominated regions using a turbulent jet positioned vertically and shooting upward for cases of various Froude numbers ( $Fr = 268, 152, 99$  and  $58$ ) and concluded that for Froude numbers bigger than  $Fr = 286$  buoyancy generated forces are small. They also concluded that hydrogen jets show similar behaviour as jets of helium and conventional hydrocarbon fuels. In the present study, helium was selected as the working fluid, because it is inert and its molecular weight is very close to the molecular weight of hydrogen.

The buoyant jet discharge flow configuration becomes more complicated by introducing a moving ambient which can be in the same direction of the discharge, opposite direction, perpendicular or at some intermediate angle. In all these cases, the flow near the release source is usually weakly advected and momentum fluxes are dominant. Farther downstream, the flow is strongly advected and the entrained ambient momentum flux dominates. Among these flow configurations, the cross-flowing turbulent jet, in which a round jet is injected into a perpendicular fluid stream, is of particular interest, as it is representative, for instance, of the dispersion of hydrogen in a windy environment.

In this study, dispersion of a buoyant, turbulent, round jet in a quiescent and moving ambient at a wide range of Froude numbers was investigated. The moving ambient was oriented perpendicular to the discharge in direction parallel to the buoyant forces. Schematic diagrams of the resulting vortical structures of the cross-flowing jet and the corresponding coordinate system are illustrated in Figure 1. The downstream distance,  $s$ , is measured along the centerline of the jet which was defined according to the procedure described in section 3.1 (see Figure 1).

Experimental evidence show that this kind of flow structure is extremely sensitive to the ratio of jet to cross-flow momentum ( $r = \rho_j U_{oc}^2 / \rho_\infty v_\infty^2$ ), and the complexity of the resultant flow structure makes it difficult to draw general conclusions about the flow configuration [7]. In most cases, the initial momentum flux of the discharge determines whether a two-dimensional or a three-dimensional flow structure is created. The experimental data suggest that if the initial momentum flux acts in the same plane as the buoyancy-generated and ambient entrained momentum flux, the resulting flow structure will have a two-dimensional trajectory [8]. The vortical structure of the turbulent cross-flowing jet

have been studied extensively, and many experiments have been conducted using different velocity ratios ( $r$ ) spanned from 5 to 35 [9]. Detailed measurements of turbulence stresses were also reported for flows with  $r = 0.5, 1$  and  $2$  [10], leading to the conclusion that the presence of a cross-flowing ambient strongly affects the jet velocity profiles.

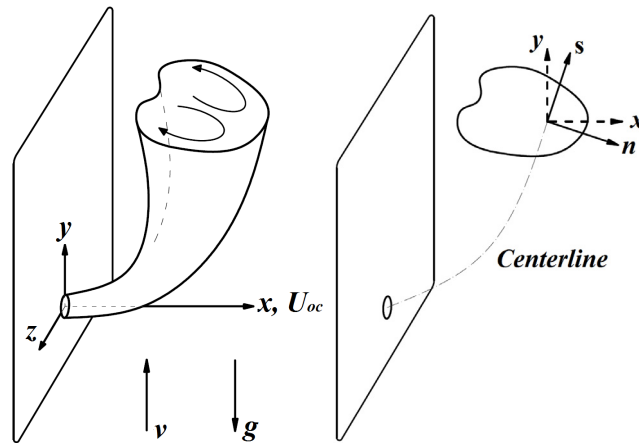


Figure 1. The vortical structure of the cross-flowing jet (left), jet coordinate system (right)

Off-centerplane measurements and the effects of different initial condition in cross-flowing jet also point to the conclusion that the flow structure is very similar to that of pure jet in momentum-dominated region of the jet, and that the complex flow structure in the jet downstream is symmetric [7]. In present study, cross-flow velocity was kept constant, and the resulting  $r$  values spanned from 0.6 to 11 for different Froude numbers considered.

This work follows two primary objectives. The first objective is to experimentally characterize the effects of buoyancy and cross-flow on hydrogen dispersion with the aim of better understanding of flow structure and flammable envelopes for uncontrolled leaks with different flow rates. Over the recent years, hydrogen leakage scenarios have been a subject of many CFD studies (e.g. [2]) and a necessary step towards validation and development of these CFD models is to have a detailed well defined experimental database. So the second goal of the present study is to provide a well-defined quantitative database that can be used for future concentration measurements and also to validate CFD models related to hydrogen release scenarios. This study focuses on the investigation of jets produced by a high-velocity gas entering a quiescent and moving ambient which emulates the unintended hydrogen leak from a high pressure system, a possible scenario for fuel cell vehicles and hydrogen stations. This type of flow is usually turbulent, unsteady and can have significant compressibility effects. In order to achieve a better understanding of the physics associated with the development of a turbulent jet, a quantitative flow visualization was accomplished by employing digital particle imaging velocimetry (DPIV). Measurements of the mean and the fluctuating velocity components along the centerline are presented for better understanding of effects of buoyancy and cross-flow.

## 2.0 EXPERIMENTAL DETAILS

### 2.1 Inflow configuration

According to Townsend [11], turbulent flows show a self-similarity when they become asymptotically independent of initial condition. However, George [12] showed analytically that entire turbulent flow is influenced by initial condition. It was concluded that different initial conditions will lead to different self-similar states in the downstream locations. Three different nozzle configurations, which are commonly used in turbulent flow studies using round jets, are smoothly contracting (contoured) nozzles, long pipes, and orifice plates. Among those, contoured nozzles has been widely used in most fundamental studies (e.g. [13,14]) because they produce a fairly uniform velocity profiles, also

referred to as top-hat profiles, with low mean initial turbulence intensity ( $\langle u' \rangle(y)/U_{oc}$ ) of about 0.5% except at edges ( $y > 0.45D$ ) [15]. This property of contoured nozzles makes them ideal for computational model validations. A long pipe located upstream of the circular orifice has also been considered widely in numerous studies (e.g. [16]). Although the exit velocity profile of circular jets issued by pipes is not uniform, the lower manufacturing cost and simplicity made long pipe inlets a common choice in fluid dynamics experiments. These pipes are usually manufactured long enough to produce a fully developed turbulent boundary layer at the exit and their mean initial turbulence intensity has been reported to be between 3 to 9.5 % [15].

Limited information is available regarding circular jets originated from sharp-edged plate nozzles. This inflow configuration is characterized by a relatively complex initial velocity profile and near-field flow structure. However, it can be argued that sharp-edged orifice plates emulate unintended hydrogen leakage scenarios more realistically than the contoured nozzle and the long pipe inlet configurations. A detailed comparison between contoured nozzle, long pipe and sharp-edged plate inflow configurations and the corresponding flow structures may be found in [17, 18]. Briefly, in a sharp-edged orifice, the flow on the upstream side of the nozzle undergoes a sudden contraction which causes an initial separation in the fluid and increases mean initial turbulence intensity subsequently. This upstream lateral contraction forces flow streamlines to initially converge towards the jet exit and suddenly expand in the jet near field very close to the nozzle exit which is called “vena contracta”. The presence of the vena contracta phenomenon causes a sudden local pressure drop and leads to a local maximum in the centerline mean velocity profile, which is one of the characteristics of a sharp-edged nozzle. It has been reported by Quinn [19] that this local velocity maximum is 30% higher than centerline velocity value at nozzle exit. Saddle-backed mean velocity profile is another characteristic of the sharp-edged orifice, and the mean initial turbulence intensity is reported to be between corresponding values in contoured and pipe nozzles [15]. The centerline mean velocity decays faster as a result of the sudden expansion and increased entrainment as the jet travels downstream from the sharp-edged orifice.

## 2.2 Experimental Setup

One of the main objectives of the current study is to document the effects of a moving ambient on the buoyant jet discharge. In this study, the jet apparatus was oriented horizontally in order to capture the buoyant characteristics of the flow. The cross-flow assembly was positioned to amplify the jet flow in the direction where the buoyancy effects were dominant. A small blower-type cubic wind tunnel with side of 18cm was designed and used for this purpose. The upper face was covered with a regular hexagon honeycomb with side of 2.5mm and the isentropic turbulence distance after honeycomb structure was calculated to be approximately 10cm. The resultant cross-flow velocity magnitude was measured to be 11m/s with the maximum of 4% variation throughout the domain. The turbulence intensity generated by the blower at nozzle tip was measured to be approximately 2% of mean cross-flow velocity. The jet issued from the wall with 24cm×26cm dimension in ( $y, z$ ) plane. The nozzle centered the wall in  $z$  direction at 10cm above the honeycomb surface (see Figure 2).

The experiments were performed using a jet apparatus consisting of a honeycomb settling chamber and a sharp-edged orifice with the edge angle of 45° (see figure 2). The exit nozzle diameter is 2mm (D) and helium were supplied by a T-cylinder monitored through mass flow controllers and exhausted horizontally to the quiescent and moving ambient for free and cross-flow jet cases respectively. Quantitative flow visualization was conducted using PIV. Detailed background information about PIV may be found in [20]. The helium flow was seeded with olive oil droplets (LaVision Aerosol Generator) serving as tracers, with a typical diameter of approximately 1 $\mu$ m. Dual head Nd: YAG laser was used to illuminate the flow tracers. The laser beam was transformed to a light sheet with approximate thickness of 500 $\mu$ m. A high resolution charge-coupled device (CCD) camera was positioned perpendicular to the light sheet in order to capture the scattered light from the illuminated particles. A schematic representation of the experimental setup is shown in Figure 2. The camera had a total of 1376 × 1040 pixels and was equipped with a 60-mm lens. The field of view of the camera corresponded to a 21.5 × 15 mm window. The imaging planes were parallel to the centre plane of the

jet in areas extended from jet exit to far field region. For calculation of the velocity field, the image area was divided into interrogation windows that were analyzed individually to yield local velocity values in the corresponding area.

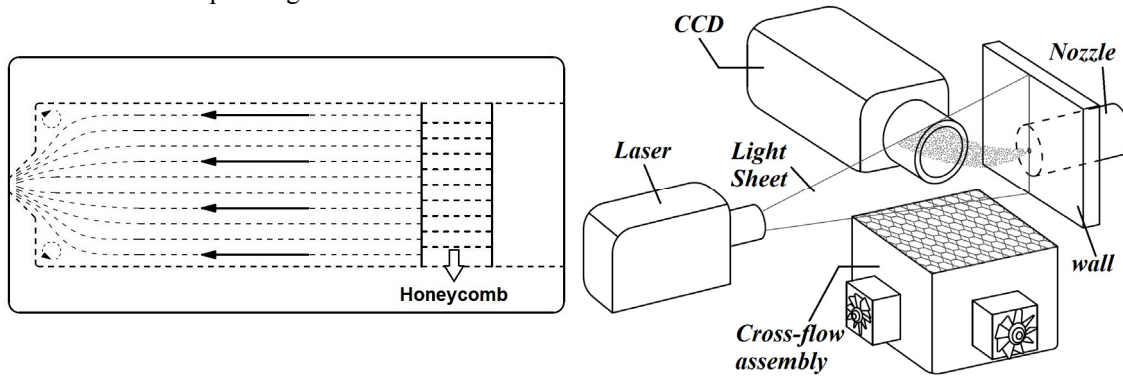


Figure 2. Nozzle schematics (left), experimental setup schematics (right)

The maximum framing rate of the camera was 15Hz, corresponding to 7.5 cross-correlated PIV images per second. Due to data transfer limitations this rate was further reduced to 4.9Hz. Lavisision DaVis 7.1 software was used to calculate global instantaneous flow velocity fields of acquired images followed by a multi-pass spatial resolution improvement process with incremental decrease of interrogation window size from  $32 \times 32$  pixels to  $16 \times 16$  pixels and with a 50% overlap in the x- and y-directions. The final spatial resolution of  $256 \times 256 \mu\text{m}$  and the temporal resolution of 4.9 Hz of the PIV image sequence were appropriate for capturing random samples for the calculation of the averaged turbulence statistics. Depending on the complexity of the resultant flow structure a total of 50 to 400 images were acquired for each case under consideration.

Table 1 represents the cases and flow conditions that were considered in this study. Volumetric flow rates together with centerline exit velocity of the jet are also given in this table for the considered geometry. Froude number has been proved to be a good measure of ratio of momentum to buoyancy forces in subsonic discharge of flows in quiescent or relatively slow flowing fluid when the density difference between two fluids is considerable. A wide range of Froude numbers was considered (i.e.  $Fr=50, 250, 500, 750$  and  $1000$ ) and experimental conditions were set accordingly. Resultant experimental Froude numbers and the corresponding Reynolds numbers at jet exit were calculated considering the jet geometry and are shown in Table 1. It should be noted that flow structure in a turbulent jet ranges from laminar ( $Re<500$ ) to transitional ( $885<Re<1360$ ) to fully turbulent ( $Re>2384$ ). The following relation was used to calculate Froude number:

$$Fr = U_{oc} / (gD(\rho_{\infty} - \rho_j) / \rho_j)^{1/2}, \quad (1)$$

where  $Fr$  – Froude number, Dimensionless;  $U_{oc}$  – Jet centerline exit velocity, m/s;  $g$  – acceleration due to gravity,  $\text{m}^2/\text{s}$ ;  $D$  – Jet diameter, mm;  $\rho_{\infty}$  – Ambient air density,  $\text{kg}/\text{m}^3$  and  $\rho_j$  – Jet exit density of helium,  $\text{kg}/\text{m}^3$ .

Table 1. Flow conditions

Case	Q (lpm – H <sub>2</sub> )	U <sub>oc</sub> (m/s)	Fr	Re
1	64.4	318.33	910	5263
2	43.4	248.98	710	4196
3	35.7	185.23	528	3121
4	21	94.56	268	1593
5	12	18.86	54	317

Helium density and viscosity are  $0.166 \text{ kg}/\text{m}^3$  and  $1.97\text{E-}05 \text{ kg}/\text{ms}$ , respectively

These leak scenarios were considered in both the quiescent and the cross-flow conditions. All properties are referenced to the room temperature  $T = 22^{\circ}\text{C}$  ( $\pm 1$ ) and the pressure  $P = 100\text{kPa}$  ( $\pm 0.5$ ). It has been reported that at the high Froude numbers ( $Fr > 1000$ ), leaks are momentum-dominated, while for the low Froude numbers, buoyancy forces are dominant, and all discharges with intermediate Froude numbers ( $1000 > Fr > 50$ ), are influenced by both the initial momentum of the jet and the buoyant forces generated by the relative density differences between the jet and the ambient gas [5]. Also, it has been reported that for Froude numbers bigger than  $Fr > 286$  buoyancy forces are negligible [6]. In the present study, helium was used as the working fluid to simulate the hydrogen dispersion; however, the density of hydrogen is approximately one half of helium density under the same conditions. Therefore, the effect of the Froude number on the buoyancy is expected to be more pronounced in the case of the hydrogen dispersion.

### 3.0 RESULTS AND DISCUSSION

#### 3.1 Jet centerline

Due to the bifurcated structure of the buoyancy-dominated flow discharges and the flows in cross-flow, the centerline of the jet was identified as shown in Figure 1, by fitting a least-square curve along the entire domain of consideration trough locus of points of maximum mean velocity.

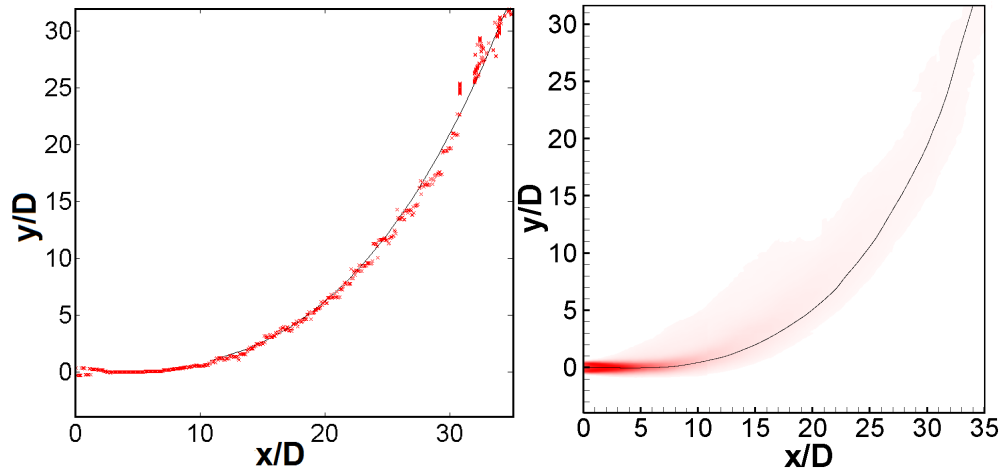


Figure 3. Local maxima in the normalized mean velocity field (left); jet centerline (right)  $Fr=1000$

The procedure of finding these local maximum points are different for the cases of jets in quiescent and cross-flow. For jet discharge in a uniform cross-flow, these local maximum points were defined in a systematic manner by first determining the points of maximum mean velocity magnitude (i.e.  $\langle |U| \rangle$ ) along x-direction in jet near field and maximum mean cross-flow-subtracted velocity magnitude (i.e.  $\langle |U - v_{\infty}| \rangle$ ) along y-direction in far field region of the flow. For the cases of the free jet discharge in quiescent ambient, the local maximum points of the mean velocity magnitude were considered in both x- and y-directions, where x-direction is parallel to jet center axis and y-direction represents the direction of cross-flow. Figure 3 represents the points of local maximum for the case of jet discharge in cross-flow for Froude number 1000 and corresponding jet centerline representation as an example. The solid black line is least squares fit to the data.

Jet centerlines corresponding to different cases considered in this study are presented in Figure 4. For cases of the jets in the quiescent ambient at high Froude numbers (i.e.  $Fr > 268$ ), effects of buoyancy were negligible, and the centerline followed an almost straight pass with no deviation. However, at low Froude numbers (i.e.  $Fr < 268$ ), jet structure was divided into a momentum and buoyancy dominated regions in the jet near- and the far-field areas, respectively. This bifurcated behavior was more pronounced at  $Fr = 50$  free jet case, where the centerline of the jet deviated from the nozzle

centerline by almost five nozzle diameters. In the cross-flow jets, flows with lower Froude numbers penetrated less in the cross-flow structure as result of lower initial jet exit momentum. Low jet to cross-flow velocity ratio for  $Fr = 50$  resulted in a sudden breakdown of the jet structure which led to appearance of a plume-like region downstream of a very short ( $x/D=1.5$ ) momentum-dominated area.

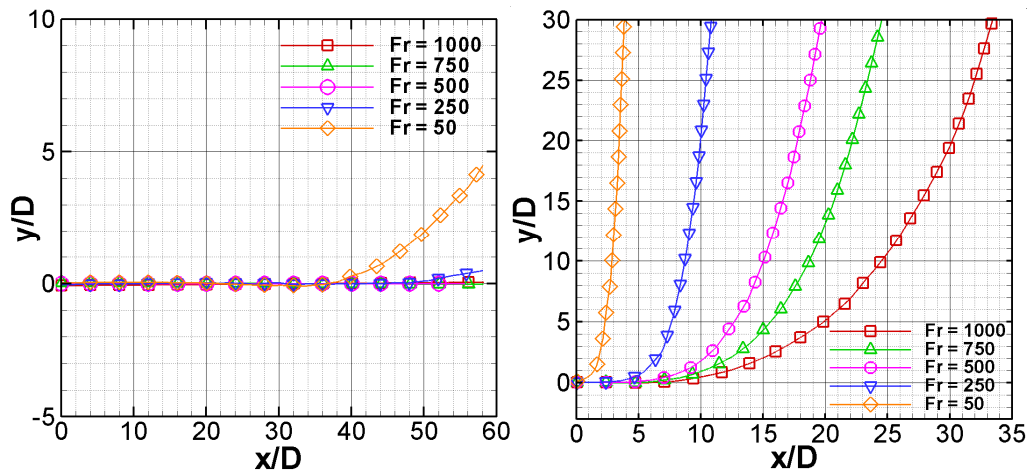


Figure 4. Jet centerlines, free jet (left), cross-flow jet (right)

### 3.2 Velocity field

Normalized mean velocity contours of free jets for different Froude numbers are shown in Figure 5.

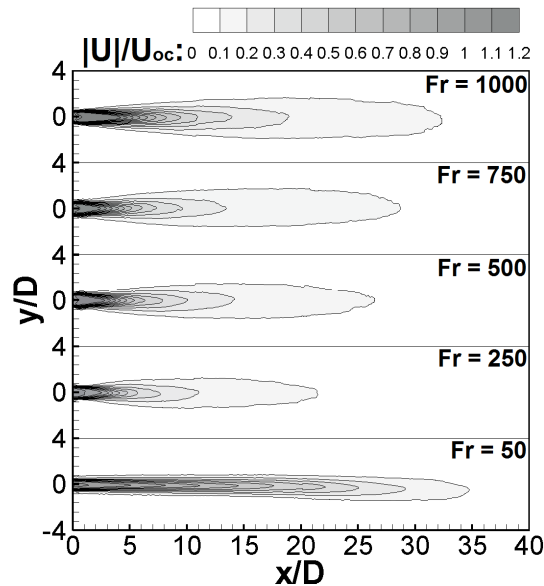


Figure 5. Normalized mean velocity magnitude contours – Free jet

For each case, the dark central areas correspond to the potential core with approximately uniform mean velocity. In the free jet cases, flow contours spread out gradually and symmetrically for cases with high Froude numbers (i.e.  $Fr > 268$ ), and the effects of buoyancy forces are negligible. However, for lower Froude numbers, the far-field region deforms under the influence of buoyancy forces which leads to lower velocity decay profiles due to buoyancy driven acceleration component and higher mixing rate. It should be noted that for  $Fr=50$ , the corresponding Reynolds number is equal to 317, which corresponds to the laminar flow. It was observed that for  $x/D < 25$ , the jet travelled with

minimal entrainment and very low decay rate but at  $x/D > 30$ , the velocity profiles decayed gradually, and high amount of mixing occurred.

As mentioned before, in jets with  $Fr < 268$ , the near-field buoyancy-dominated regions were observed. To distinguish the momentum- and buoyancy-dominated regions in the jet, the jet/plume characteristic length scale,  $L_M$ , which describes the relative importance of momentum and buoyancy fluxes [21], was used. Simplified version of this characteristic length scale is given in following relation.

$$L_M = Fr D, \tag{2}$$

where  $Fr$  – Froude number, Dimensionless;  $D$  – Jet diameter, mm.

The dimensionless distances using  $L_M$  length scale results in very small values in momentum dominated flows versus larger span in flows with smaller  $Fr$  numbers. Figure 6 illustrates the jet centerlines for free jet cases using this length scale.

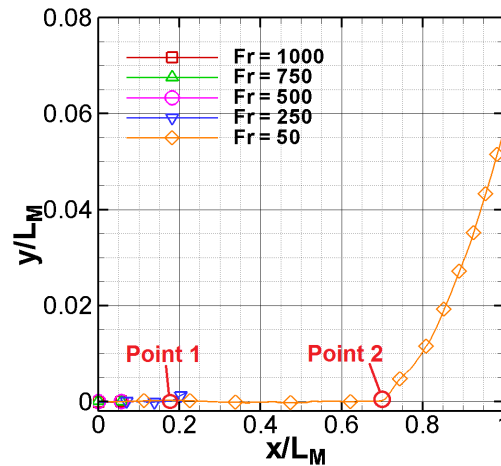


Figure 6. Jet centerline for free jet case using  $L_M$  length scale

Taking the overall jet structure shown in Figure 4 and 5 into consideration together with branch points shown in Figure 6, it was observed that first effects of buoyancy in case of  $Fr = 250$  and  $50$ , happens at approximately  $x/L_M = 0.16$  and  $0.61$  which corresponds to  $x/D = 43$  and  $32$  respectively. These branching points are identified as Points 1 and 2 in Figure 6.

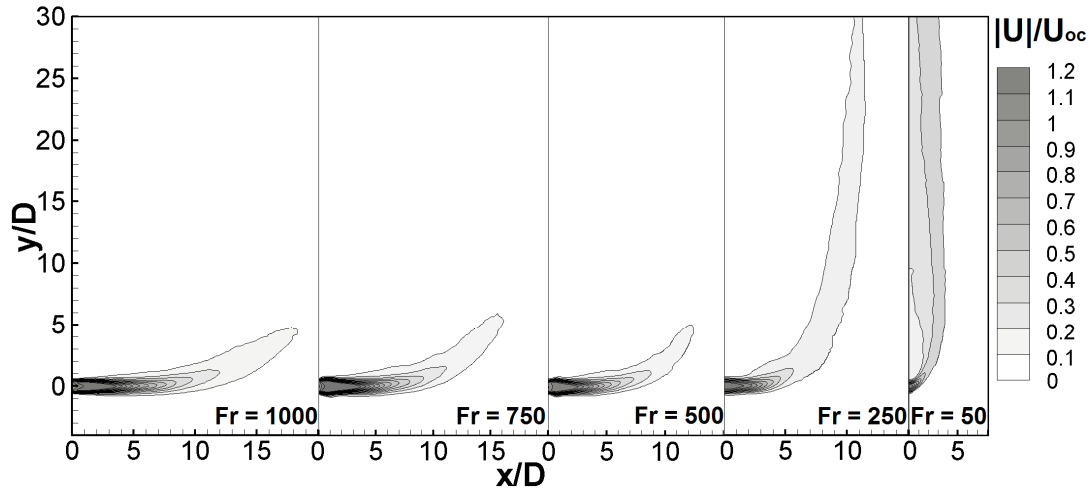


Figure 7. Normalized mean velocity magnitude contours – Jet with cross-flow

Normalized mean velocity contours for cross-flow jets are presented in Figure 7. Cross-flow velocity was kept constant for all cases, resulting in the jet-to-cross-flow velocity ratios of  $r = 11, 7, 6, 2$  and  $0.6$  for  $Fr = 1000, 750, 500, 250$  and  $50$ , respectively. The jets with the higher Froude numbers penetrated farther into the moving ambient, as it was expected.

### 3.3 Velocity decays

Normalized velocity decay profiles along the jet centerline coordinate system are presented in Figure 8. Here, centerline mean velocity magnitude,  $|U|$ , for the case of free jet and centerline mean cross-flow-subtracted velocity,  $|U-v_\infty|$ , for the case of jet in cross-flow were normalized by the mean jet exit velocity at center of the orifice,  $U_{oc}$ , and is plotted against downstream coordinate,  $s$ , normalized by jet diameter,  $D$ .

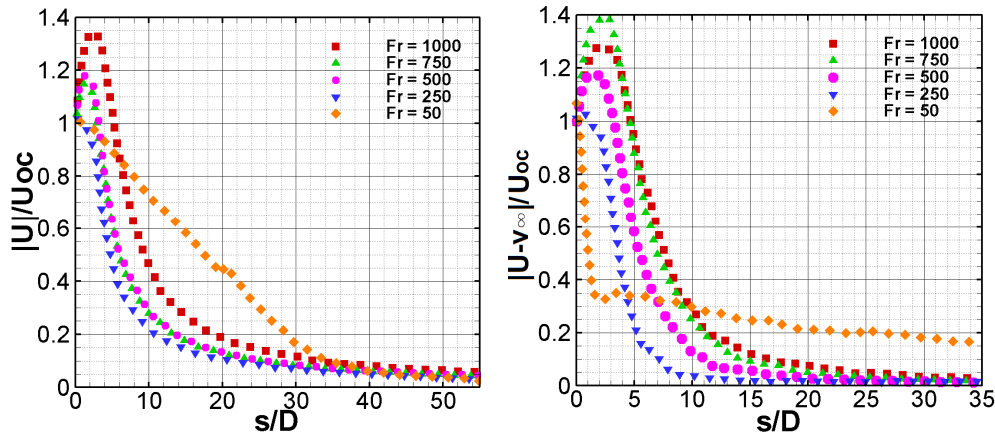


Figure 8. Normalized mean velocity decay along jet centerline, Jet in quiescent ambient (left) and jet in cross-flow (right)

Values are equal to unity at jet exit followed by a rapid increase of approximately 30% to  $U_{mc}$  because of sharp-edged orifice exit geometry as explained in section 2.1 and [19]. The decay rates were slower in the buoyancy-dominated regions as a result of the buoyancy-driven acceleration components. For the case of  $Fr = 50$ , the velocity decay rates were slower because of presence of the laminar and the plum-like flow structure in cases of the free jet and the jet in cross-flow, respectively.

The data shown in Figure 8 illustrates that in free jet cases, downstream of the potential core region, the jet velocity decreased at a high rate, with the exception of the  $Fr = 50$  case, in which the exit velocity values persisted for several nozzle diameters downstream because of the laminar nature of the flow. For higher Froude numbers, the jet spread rapidly because of the high ambient entrainment, which was enhanced by buoyancy effects. In other words, the decrease in the Froude number corresponded to faster centerline velocity decays. Similar behavior was observed in the cases of the jets discharging in the cross-flow. As it is shown in Figure 7 and 8 for jet dispersions in cross-flow, decreasing the Froude number led to a smaller potential core area because of the lower initial momentum at jet exit. It should be also noted that in the case of the lower Froude numbers, the jet spread rates increased, and the overall jet structure became unstable farther downstream as result of the higher buoyancy forces.

### 3.4 Mean velocity profiles

The initial mean normalized radial velocity profiles together with corresponding normalized root-mean-square (rms) values are shown in Figure 9.

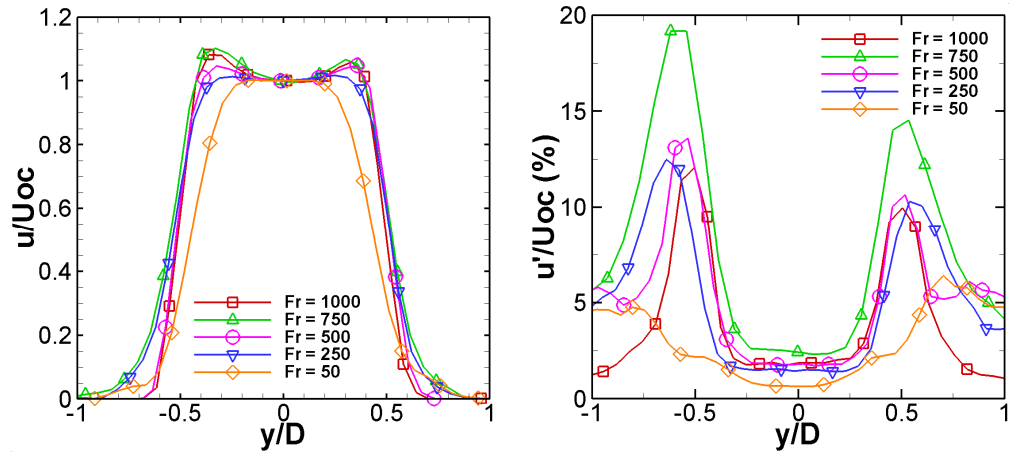


Figure 9. Initial normalized radial mean velocity profile (left) and normalized radial rms values (right)

As also shown in sections 3.2 and 3.3, for the cases of  $Fr > 250$ , the increase in the Froude number leads to a larger potential core area and a more pronounced saddled-back initial velocity profile as a result of the higher initial momentum, which moves the point of the vena-contracta further downstream and causes a higher peak in centerline velocity profile. On the other hand, decreasing the Froude number moves the vena-contracta point towards the jet exit, which leads to a top-hat initial velocity profile and lower initial turbulent intensity. The data are in a good agreement with the results reported in [17].

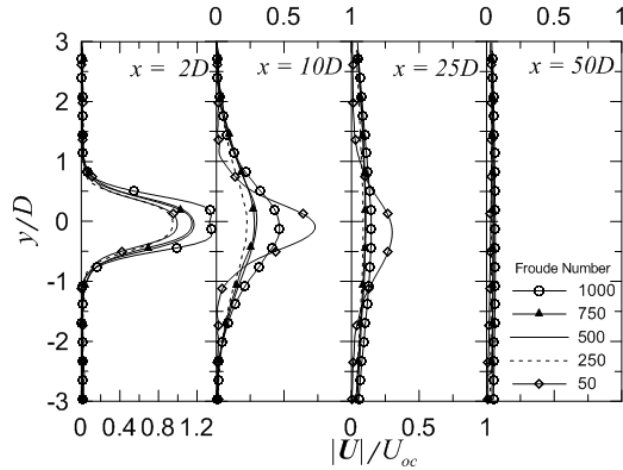


Figure 10. Mean normalized velocity magnitude profiles of the free jet case

Figure 10 presents the normalized mean velocity magnitude profiles for the free jet discharge at several downstream locations. In the cases with high Froude number, radial velocity profiles show a symmetrical bell-shaped peak which coincides with the jet centerline. However, in the case of low Froude numbers, these symmetrical velocity profiles started to deform and shift up farther downstream because of the presence of strong buoyancy forces. For case of jet in cross-flow, further analysis taking account of the shift of the center of the jet due to cross-flow is required to allow a better comparison of the various Froude numbers.

### 3.5 Turbulence quantities

Normalized rms velocity components along jet center coordinate system are plotted in Figure 11. Velocity fluctuations had low initial values because of the sharp-edged orifice of the jet apparatus as

mentioned in previous section. In the cases of the jets in quiescent ambient, these velocity fluctuations increased rapidly downstream of the potential core region. Axial fluctuations were generally higher than the radial fluctuations for all cases considered herein. At low Froude numbers (i.e.  $Fr < 268$ ), the velocity fluctuations increased in the buoyancy-dominated flow region in free jet cases. It should be noted that for  $Fr = 50$ , as a result of laminar nature of the flow in jet near-field, the velocity fluctuation values were very low which gradually increased in the transition region.

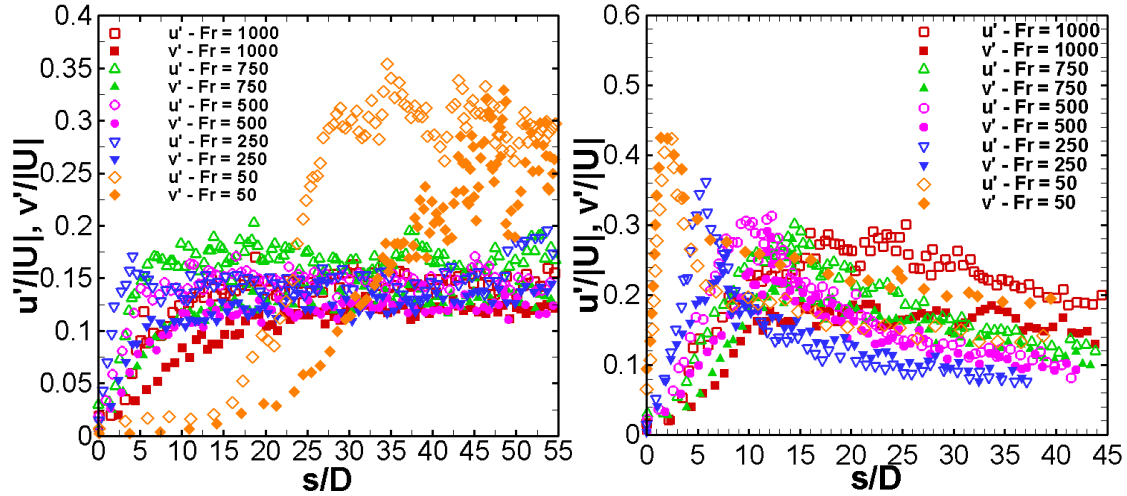


Figure 11. Normalized velocity fluctuations along jet center line, free jet (left), jet in cross-flow (right)

Figure 11 also shows velocity fluctuation values for jet discharge in cross-flow. Similar to free jet case because of sharp-edged orifice nozzle structure, these variations had a small initial value and increased in the potential core area. The increasing rates in potential core areas are slower comparing to cases of jets in quiescent ambient. These rms values were generally substantially higher in presence of the cross-flow. Similar to jet in quiescent ambient, in cross-flowing jets, axial fluctuations were generally higher than the radial fluctuations for all cases considered in potential core area and also farther downstream in cases with high Froude numbers. Decrease in the Froude number led to higher fluctuations because of presence of higher buoyancy forces. In jet downstream locations where buoyancy forces are more pronounced, radial fluctuation values increase noticeably.

As shown in the figure lowering the Froude number led to presence of a peak in rms plots in the potential core region. For free jet cases this peak is evident in case of  $Fr = 250$  in axial fluctuation plot. For the cases of jet in cross-flow this peak is more evident and it is more pronounced in cases with lower Froude numbers.

#### 4.0 CONCLUSIONS

Effects of buoyancy and cross-flow were investigated in subsonic release of buoyant gas in quiescent and cross-flow using helium discharged from a sharp-edged orifice round jet. Velocity fields were obtained using PIV for a wide range of Froude numbers. Mean and fluctuation velocity components were presented to quantify the effects of buoyancy forces and it was shown that lowering the Froude number led to slower velocity decays due to the buoyancy-driven acceleration components in buoyancy dominated regions. Increasing effects of buoyancy were observed by reducing the Froude number. For the cases with  $Fr < 268$ , the buoyancy forces were more pronounced in jet far-field regions. The flow conditions selected in the study correspond to a range of situations involving hydrogen release. The present data can serve to validate computational models derived for investigating hydrogen safety scenarios [2].

## Acknowledgments

Supports of NSERC Hydrogen Canada (H2Can) are gratefully acknowledged.

## References

1. Jirka, G.H. "Integral model for Turbulent Buoyant jets in Unbounded Stratified Flows Part 1: Single Round Jet." *J. Env. Fluid Mech.*, **4**, 2004, pp. 1-56.
2. B. Chernyavsky, T.C. Wu, F. Peneau, P. Benard, P. Oshkai, N. Djilali. "Numerical and experimental investigation of buoyant gas release: Application to hydrogen jets." *Int. J. Hydrogen Energy*, **36**, No. 3, 2010, pp. 2645-2655.
3. R.W. Schefer, W.G. Houf, B. Bourne, J. Colton. "Spatial and radiative properties of an open-flame hydrogen plume." *Int. J. Hydrogen Energy*, **31**, No. 10, 2006, pp. 1132-1140.
4. R.W. Schefer, W.G. Houf, T.C. Williams, B. Bourne, J. Colton. "Characterization of high-pressure, under expanded hydrogen jet flames." *Int. J. Hydrogen Energy*, **32**, No. 12, 2007, pp. 2081-2093.
5. R.W. Schefer, W.G. Houf, T.C. Williams. "Investigation of small scale unintended release of hydrogen: buoyancy effects." *Int. J. Hydrogen Energy*, **33**, No. 17, 2008, pp. 4702-4712.
6. R.W. Schefer, W.G. Houf, T.C. Williams. "Investigation of small-scale unintended release of hydrogen: momentum dominated regime." *Int. J. Hydrogen Energy*, **33**, No. 21, 2008, pp. 6373-6384.
7. L. K. Su, M. G. Mungal. "Simultaneous measurements of scalar and velocity field evolution in turbulent crossflowing jets." *J. Fluid Mech.*, **513**, 2004, pp. 1-45.
8. Kikkert, Gustaaf Adriaan. *Buoyant Jets with Two and Three Dimensional Trajectories*. PhD Thesis, Christchurch, New Zealand: University of Canterbury, 2006.
9. Crabb, D., Durao, D. F. G. & Whitelaw, J. H. "A round jet normal to a crossflow." *J. Fluids Eng.*, **103**, 1981, pp. 142-153.
10. Andreopoulos, J. & Rodi, W. "Experimental investigation of jets in a crossflow." *J. Fluid Mech.*, **138**, 1984, pp. 93-127.
11. Townsend, A.A. *The structure of turbulent shear flow, 2nd edition*. Cambridge University press, 1996.
12. George, W.K. *The Self-Preservation of turbulent flows and its relation to initial condition and coherent structures*. Ed. Arndt, R.E.A and George, W.K., 1989.
13. S.C. Crow, F.H. Champagne. "Orderly Structure in Jet Turbulence." *J. Fluid Mech.*, **48**, 1971, pp. 547-591.
14. H.A. Becker, H.C. Hottal, G.C. Williams. "The Nozzle fluid Concentration field of the round, turbulent, free jet." *J. Fluid Mech.*, **30**, 1967, pp. 285-303.
15. E.J. Smith, J. Mi, G.J. Nathan and B.B. Dally. "Preliminary Examination of a "Round jet initial condition anomaly" for k-e Turbulent Model." *15th Australasian Fluid Mech. Conference*. Sydney: The University of Sydney, 2004.
16. F.C. Lockwood, A. Moneib. "Fluctuating Temperature Measurements in heated round free jet." *Combust. Sci. Technol.*, **22**, 1980, pp. 63-81.
17. J. Mi, G.J. Nathan and D.S. Nobes. "Mixing characteristics axisymmetric free jets from a contoured nozzle, an orifice plate and a pipe." *J. Fluid Eng.*, **123**, No. 4, 2001, pp. 878-883.
18. G.J. Nathan, J. Mi, G.J. R. Newbold, D.S. Nobes and Z.T. Alwahabi. "Effects of subtle and dramatic changes to initial conditions on a jet's turbulent structure, mixing and combustion." *15th Australasian Fluid Mechanics Conference*. Sydney: The University of Sydney, 2004.
19. Quinn, W.R. "Turbulent free jet flows issuing from sharp-edged rectangular slots: the influence of slot aspect ratio." *Exp. Therm. Fluid. Sci.*, **5**, No.2, 1992, pp. 203-215.
20. Adrian, R. "Particle-Imaging Techniques for Experimental Fluid Mechanics." *Annual Review Fluid Mechanics*, **23**, No.1, 1991, pp. 261-304.
21. List, P. N. Papanicolaou And E. J. "Investigation of round vertical turbulent buoyant jets." *J. Fluid Mech.*, **195**, 1988, pp. 341-391.